Dalton Transactions

ROYAL SOCIETY OF CHEMISTRY

PAPER

View Article Online
View Journal | View Issue

Cite this: *Dalton Trans.*, 2024, **53**, 1977

Mitochondria-targeted neutral and cationic iridium(III) anticancer complexes chelating simple hybrid sp^2-N/sp^3-N donor ligands†‡

Pengwei Li, Lihua Guo, * Jiaxing Li, Zhihao Yang, Hanxiu Fu, Kangning Lai, Heqian Dong, Chunyan Fan and Zhe Liu *

Most platinum group-based cyclometalated neutral and cationic anticancer complexes with the general formula $[(C\hat{}N)_2Ir(XY)]^{0/+}$ (neutral complex: XY = bidentate anionic ligand; cationic complex: XY = bidentate neutral ligand) are notable owing to their intrinsic luminescence properties, good cell permeability, interaction with some biomolecular targets and unique mechanisms of action (MoAs). We herein synthesized a series of neutral and cationic amine–imine cyclometalated iridium(III) complexes using Schiff base ligands with sp^2-N/sp^3-N $N\hat{}NH_2$ chelating donors. The cyclometalated iridium(III) complexes were identified by various techniques. They were stable in aqueous media, displayed moderate fluorescence and exhibited affinity toward bovine serum albumin (BSA). The complexes demonstrated promising cytotoxicity against lung cancer A549 cells, cisplatin-resistant lung cancer A549/DDP cells, cervical carcinoma HeLa cells and human liver carcinoma HepG2 cells, with IC_{50} values ranging from 9.98 to 19.63 μM. Unfortunately, these complexes had a low selectivity (selectivity index: 1.62–1.98) towards A549 cells and BEAS-2B normal cells. The charge pattern of the metal center (neutral or cationic) and ligand substituents showed little influence on the cytotoxicity and selectivity of these complexes. The study revealed that these complexes could target mitochondria, cause depolarization of the mitochondrial membrane, and trigger the production of intracellular ROS. Additionally, the complexes were observed to induce late apoptosis and perturb the cell cycle in the G_2/M or S phase in A549 cells. Based on these results, it appears that the anticancer efficacy of these complexes was predominantly attributed to the redox mechanism.

Received 5th November 2023,
Accepted 12th December 2023

DOI: 10.1039/d3dt03700b

rsc.li/dalton

1. Introduction

Cisplatin and its analogues such as carboplatin and oxaliplatin are the most well-known anticancer drugs used for cancer treatment.[1] Nevertheless, the lack of selectivity, which leads to many severe side effects, and drug resistance toward cancer cells limit the use of these platinum-based anticancer drugs. To overcome these drawbacks, many alternative non-platinum-based organometallic anticancer complexes of iridium, rhodium, ruthenium, osmium, *etc.* have been developed.[2–5] Among these complexes, cyclometalated neutral and cationic iridium(III) complexes with the general formula $[(C\hat{}N)_2Ir(XY)]^{0/+}$ (neutral complex: XY = bidentate anionic ligand; cationic complex: XY = bidentate neutral ligand) were notable owing to their intrinsic luminescence properties, good cell permeability, interaction with some biomolecular targets and unique mechanisms of action (MoAs), which allowed for many applications such as bio-probes, cellular imaging reagents and highly active anticancer agents.[4,6–12] Most of these studies have been focused on the synthesis and biological evaluation of cyclometalated neutral and cationic complexes using different bidentate XY ligands, which have mostly been chosen as N^N donors (Scheme 1, **I**).

Mitochondria are essential organelles that are associated with cellular energy production. They are also involved in many other cellular activities such as the production of reactive oxygen species (ROS), disruption of mitochondrial membrane potential (MMP) and mitochondria-mediated apoptosis.[13–15] Mitochondria have been shown to be the main target for many

Key Laboratory of Life-Organic Analysis of Shandong Province, Key Laboratory of Green Natural Products and Pharmaceutical Intermediates in Colleges and Universities of Shandong Province, Institute of Anticancer Agents Development and Theranostic Application, School of Chemistry and Chemical Engineering, Qufu Normal University, Qufu 273165, P. R. China. E-mail: guolihua@qfnu.edu.cn, liuzheqd@163.com

† In honor of Professor Thomas R. Ward on his 60th birthday.

‡ Electronic supplementary information (ESI) available: Additional experimental details and methods, ^1H, $^{13}C\{^1H\}$ NMR, $^{31}P\{^1H\}$ NMR spectra, and ESI-MS spectra for all compounds (Fig. S1–S56). See DOI: https://doi.org/10.1039/d3dt03700b

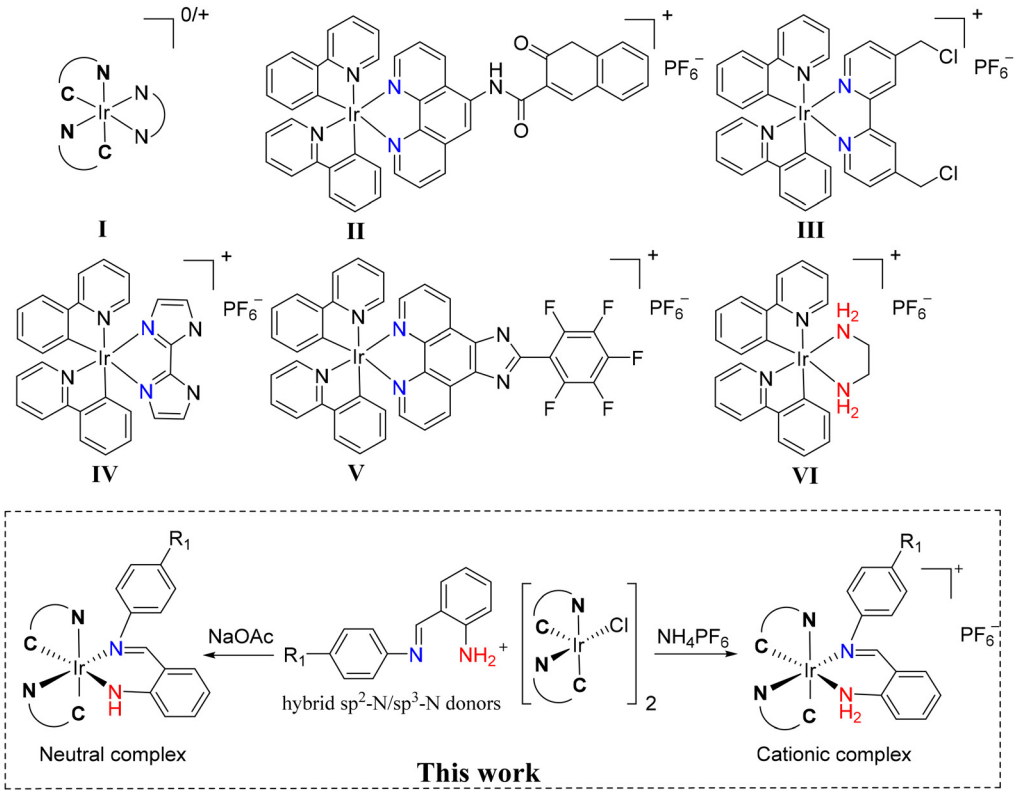

Scheme 1 The reported organometallic *N*,*N*-chelating cyclometalated complexes and our current work.

reported cyclometalated iridium(III) complexes.[16–26] For example, coumarin-appended cyclometalated iridium(III) complexes reported by the Mao group were able to target mitochondria specifically and exhibited anticancer activity by inducing morphological changes in the organelle (Scheme 1, **II**).[20] Cyclometalated iridium(III) complexes with a chloromethyl group on the bipyridine (bpy) could also target mitochondria *via* nucleophilic substitution with reactive thiols in mitochondrial proteins (Scheme 1, **III**).[22] The co-localization experiments using confocal microscopy showed that biimidazole-based iridium(III) complexes are specifically localized in the mitochondria of A549 cancer cells (Scheme 1, **IV**). The anticancer efficacy of these complexes was associated with pathways involved in the depolarization of mitochondrial membrane potential (MMP) and induction of oxidative stress.[23] The Chao group has reported several fluorinated N^N-chelating iridium(III) complexes, which can penetrate cell membranes rapidly, preferentially accumulating in mitochondria and inducing cell apoptosis *via* the mitochondrial pathway (Scheme 1, **V**).[24] Basically, drugs that target the mitochondria possess two primary features: high positive charge and strong lipophilicity.[27] Due to their higher mitochondrial membrane potential, lipophilic cations tend to accumulate more in the mitochondria of cancer cells compared to normal cells.[28] Moreover, anticancer complexes with strong lipophilic properties may disrupt normal metabolic homeostasis and intracellular ROS levels by increased binding to mitochondrial membranes.[29–31]

Notably, the coordination mode of the above-mentioned cyclometalated N,N-chelating iridium(III) complexes was sp^2-N/sp^2-N imine–metal (C=N → metal, Scheme 1, **II–V**). In contrast, the reported cyclometalated diamine-based iridium(III) complexes chelating sp^3-N/sp^3-N donor ligands (H_2N → metal, Scheme 1, **VI**) were found to be localized in the lysosomal compartments.[32] Thus, we became interested in investigating the biological behavior of cyclometalated iridium(III) complexes chelating the hybrid sp^2-N/sp^3-N donor ligands. Herein, we synthesized a series of neutral and cationic amine–imine cyclometalated iridium(III) complexes using Schiff base ligands with sp^2-N/sp^3-N N^NH_2 chelating donors (Scheme 2). It was surprising that this simple Schiff base has not yet been utilized in preparing cyclometalated platinum group-based complexes. These novel neutral and cationic cyclometalated complexes exhibited potent anticancer activity towards several cancer cell lines and could overcome platinum resistance. In particular, their possible MoAs such as mitochondria-targeting, ROS overproduction and cell apoptosis have also been studied.

2. Results and discussion

2.1. Synthesis and characterization

Ligands **L1–L3** can be easily prepared from a single-step acid-catalyzed reaction.[33,34] This kind of simple ligand offers a versatile and cost-effective platform for developing new cyclome-

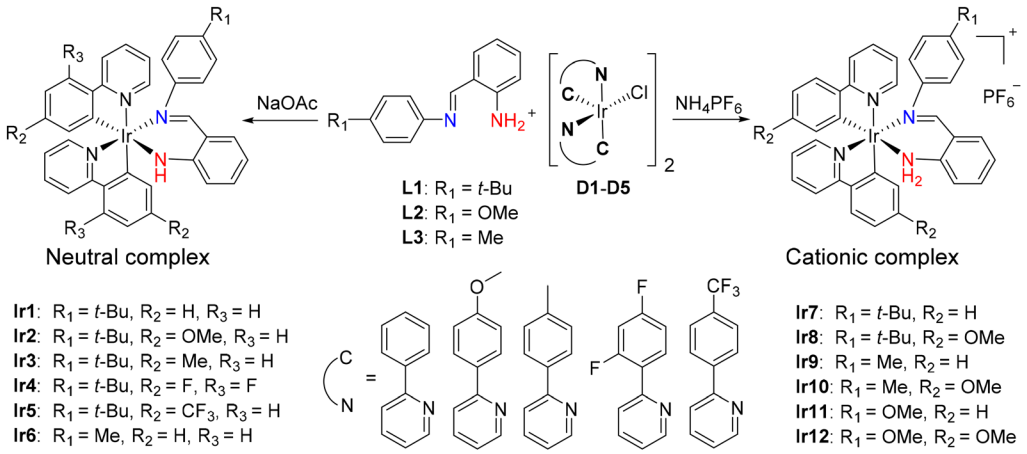

Scheme 2 Synthesis of cyclometalated iridium(III) complexes.

talated platinum group metal complexes chelating hybrid sp^3-N/sp^2-N donors. The cyclometalated iridium(III) precursors **D1–D5** were prepared using the reported procedures.[9,25] Treatment of **D1–D5** with sp^2-N/sp^3-N ligands **L1–L3** and a slight excess of the deprotonating agent NaOAc in CH_3OH/CH_2Cl_2 (v/v, *ca.* 1 : 1) at room temperature afforded neutral complexes **Ir1–Ir6** in 52–57% isolated yields. Meanwhile, the cationic complexes **Ir7–Ir12** as the PF_6^- salts were successfully generated in 53–56% isolated yields by the reaction of **D1** and **D2** with ligands **L1–L3** and an excess of NH_4PF_6. All of these new complexes were stable and highly soluble in common solvents like DMSO, DCM and MeOH, but poorly soluble in aqueous solution. Therefore, nontoxic amounts of DMSO were used to assist dissolution in subsequent biological experiments. Spectroscopic analysis (^{1}H, ^{13}C{^{1}H} NMR, ^{31}P{^{1}H} NMR and mass spectrometry) (Fig. S1–S42†) and CHN elemental analysis were used to determine the purity of these complexes. The ^{1}H NMR spectra of cyclometalated complexes **Ir1–Ir12** showed a characteristic peak corresponding to the C*H*=N group (neutral complexes **Ir1–Ir6**, chemical shift: 8.00–8.06 ppm; cationic complexes **Ir7–Ir12**, chemical shift: 8.15–8.32 ppm). In the ^{13}C{^{1}H} NMR spectra, the characteristic peak of **Ir1–Ir12** was at 166.31–169.76 ppm, which was assigned to the imine carbon of the *C*H=N group. The characteristic peaks of complexes **Ir7–Ir12** with the PF_6^- counteranion were found in the ^{31}P NMR spectra (Fig. S15, S18, S21, S24, S27 and S30†), suggesting the cationic structure of these complexes. Unfortunately, multiple attempts to obtain single crystals of these neutral and cationic complexes have failed.

2.2. Absorption and emission spectroscopy

The UV-vis absorption spectra of **Ir1–Ir12** in MeOH solutions at 37 °C are shown in Fig. 1a. All of these cyclometalated iridium(III) complexes exhibit strong absorption bands at <300 nm, which were associated with spin-allowed π–π* electronic ligand-centered (LC) transitions. The broad bands in the range of 300–360 nm were attributed to amine–imine π–π* ligand-centered charge transfer (LCCT) and metal-to-ligand

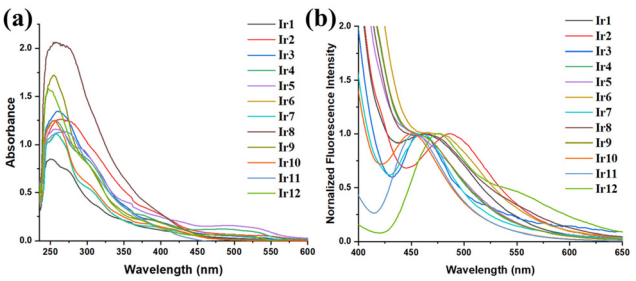

Fig. 1 (a) The UV-visible absorbance spectra of **Ir1–Ir12** (20 μM) in MeOH solutions at 37 °C. (b) Normalized emission spectra of **Ir1–Ir12** (20 μM) in MeOH at 37 °C (**Ir1–Ir12**: λ_{ex} = 388 nm).

charge transfer (MLCT) transitions. Furthermore, the broad and less intense bands at >360 nm were attributed to singlet and triplet MLCT transitions. The absorption behavior of these complexes was similar to that of previously reported cyclometalated iridium(III) complexes.[6,35,36]

Upon excitation at λ_{ex} = 388 nm, **Ir1–Ir12** exhibited emission maxima (λ_{em}) ranging from 450 to 485 nm in MeOH at 37 °C (**Ir1**: 463 nm, **Ir2**: 485 nm, **Ir3**: 461 nm, **Ir4**: 456 nm, **Ir5**: 452 nm, **Ir6**: 473 nm, **Ir7**: 459 nm, **Ir8**: 463 nm, **Ir9**: 455 nm, **Ir10**: 450 nm, **Ir11**: 474 nm, **Ir12**: 475 nm). These emission spectra showed strong similarity among the complexes, indicating that the charge pattern of the metal center (neutral or cationic) and ligand substitution had little effect. The relative emission quantum yields (Φ) of these complexes in EtOH solutions were measured using fluorescein as the standard (**Ir1**: 0.243, **Ir2**: 0.156, **Ir3**: 0.160, **Ir4**: 0.156, **Ir5**: 0.214, **Ir6**: 0.167, **Ir7**: 0.140, **Ir8**: 0.099, **Ir9**: 0.144, **Ir10**: 0.159, **Ir11**: 0.096, **Ir12**: 0.115). Moreover, the average fluorescence lifetime of these complexes ranged from 1.02 to 2.47 ns (Fig. S43†) (**Ir1**: 2.08 ns, **Ir2**: 2.34 ns, **Ir3**: 2.47 ns, **Ir4**: 1.19 ns, **Ir5**: 1.06 ns, **Ir6**: 2.19 ns, **Ir7**: 1.06 ns, **Ir8**: 1.59 ns, **Ir9**: 1.02 ns, **Ir10**: 1.03 ns, **Ir11**: 1.67 ns, **Ir12**: 1.60 ns), indicating that these complexes were fluorescent. Similar fluorescence behavior has been observed in many other cyclometalated iridium(III) complexes.[6,35,36] The

photoluminescence characteristic of these complexes can facilitate the exploration of MoAs by bio-imaging analysis.

2.3. Solution stability

The stability of **Ir1–Ir12** in 10% DMSO and 90% PBS (pH ≈ 7.4, prepared from H_2O) was monitored by UV-vis spectroscopy at 37 °C over 24 hours. No change or only minor changes in the absorption spectra of **Ir1–Ir12** were observed, which confirmed their stability in diluted solutions with a high content of water (Fig. S47†). We also measured the stability of **Ir1**, **Ir8** and **Ir9** using ^{1}H NMR at 37 °C in 75% DMSO-d_6 and 25% PBS (pH ≈ 7.4, prepared from D_2O) for 24 hours. No additional peaks were found in the ^{1}H NMR spectra (Fig. S44–S46†). This result further indicated that the complexes were stable and no decomposition occurred under these conditions. Overall, these complexes were found to be relatively stable, which was similar to the reported N,N-chelating cyclometalated iridium(III) complexes.[6] Thus, the complexes in this system were suitable for further investigation of anticancer activities under aqueous conditions.

2.4. Cytotoxicity

The MTT assay was used to evaluate the effect of **Ir1–Ir12** on the viability of A549 lung cancer cells, A549/DPP cells (cisplatin-resistant), cervical carcinoma HeLa cells, human hepatocellular liver carcinoma HepG2 cells and noncancerous BEAS-2B cells with clinical cisplatin as the control. The cyclometalated precursors and the free ligands showed very low cytotoxicity against A549 and HeLa cells, with IC_{50} values above 100 μM (Table S1†). Surprisingly, **Ir1–Ir12** exhibited significant cytotoxicity against A549 cells (13.58–16.32 μM), A549/DDP cells (15.04–19.63 μM), HeLa cells (9.98–13.24 μM) and HepG2 cells (14.29–19.21 μM), which were on par with or even better than clinical cisplatin. In particular, **Ir1–Ir12** were 1.4–1.7 times more potent than cisplatin against A549 cancer cells (13.58–16.32 μM *vs.* 23.06 μM). These complexes also exhibited high cytotoxicity against cisplatin-resistant A549/DPP cells (15.04–19.63 μM), indicating a different mechanism of action with cisplatin. However, the structure–activity relationship in this system was not obvious. The charge pattern of the metal center (neutral or cationic) and the type of ligand had little effect on the cytotoxicity of these complexes. Unfortunately, all of the iridium(III) complexes were still active towards BEAS-2B cells and had low selectivity toward A549 cancer cells over BEAS-2B normal cells with selectivity index (SI) values ranging from 1.62 to 1.98 (Table 1).

2.5. Protein binding studies

To comprehend the function of anticancer complexes in cells, it is crucial to analyze their interactions with proteins. Serum albumin, the most abundant protein in blood, delivers hydrophobic complexes to cells. Herein, bovine serum albumin (BSA) was used instead of human serum albumin (HSA) since it has a similar structure and is readily available. The fluorescence of BSA mainly originates from two protein residues: tyrosine (Tyr) and tryptophan (Trp). The binding strengths of **Ir1** and **Ir7** with BSA were evaluated using UV-vis absorption and fluorescence spectra (Fig. S48†). As the concentrations of complexes **Ir1** and **Ir7** increased, the fluorescence intensity of BSA decreased steadily at 353 nm, indicating that the complexes interacted with BSA in a static quenching mode. Synchronous fluorescence spectroscopy is a useful technique for studying conformational changes in BSA upon the addition of the complexes. The emission wavelength of Tyr decreased at 287 nm ($\Delta\lambda$ = 15 nm) with a slight red shift of 1 nm, while the emission wavelength of Trp decreased at 276 nm ($\Delta\lambda$ = 60 nm) with an obvious red shift of 4 nm (Fig. S49†). These results suggested that **Ir1** and **Ir7** primarily affect the conformation of the Trp microregion during the binding process with BSA.

2.6. Cellular uptake pathway

Due to the fluorescence properties of these cyclometalated complexes, we also investigated the cellular uptake mechanism of **Ir1** and **Ir7** by confocal microscopy. The uptake pathways of

Table 1 IC_{50} values of **Ir1–Ir12** tested toward cancer and normal cell lines and comparison with cisplatin

	IC_{50} (μM)					
Complexes	A549	A549/DDP	HeLa	HepG2	BEAS-2B	SI[a]
Ir1	15.68 ± 0.11	17.05 ± 0.19	11.36 ± 0.17	17.14 ± 0.07	28.74 ± 0.09	1.83
Ir2	14.18 ± 0.24	16.09 ± 0.08	10.87 ± 0.27	16.73 ± 0.24	28.09 ± 0.14	1.98
Ir3	14.22 ± 0.18	16.23 ± 0.08	11.84 ± 0.30	16.05 ± 0.17	26.69 ± 0.21	1.88
Ir4	13.97 ± 0.05	15.04 ± 0.09	10.16 ± 0.13	15.69 ± 0.22	25.42 ± 0.16	1.82
Ir5	13.58 ± 0.17	16.04 ± 0.36	11.27 ± 0.03	14.29 ± 0.27	25.04 ± 0.21	1.84
Ir6	14.36 ± 0.39	17.31 ± 0.19	10.26 ± 0.18	15.28 ± 0.19	23.26 ± 0.14	1.62
Ir7	16.32 ± 0.14	19.63 ± 0.14	11.45 ± 0.09	18.31 ± 0.13	29.62 ± 0.36	1.79
Ir8	15.41 ± 0.26	17.48 ± 0.11	10.96 ± 0.18	18.26 ± 0.11	28.47 ± 0.22	1.85
Ir9	13.98 ± 0.16	17.56 ± 0.09	9.98 ± 0.03	17.48 ± 0.18	25.44 ± 0.17	1.82
Ir10	16.09 ± 0.21	19.24 ± 0.24	13.24 ± 0.09	19.21 ± 0.20	28.15 ± 0.14	1.75
Ir11	14.28 ± 0.09	17.65 ± 0.07	10.24 ± 0.16	16.68 ± 0.33	25.18 ± 0.24	1.76
Ir12	15.69 ± 0.27	19.25 ± 0.09	11.36 ± 0.28	18.51 ± 0.17	26.18 ± 0.23	1.67
Cisplatin	23.06 ± 0.18	>100	7.84 ± 0.19	22.58 ± 0.18	39.60 ± 0.38	1.72

[a] SI: the selectivity index represents the IC_{50} ratio of BEAS-2B normal cells to A549 cancer cells.

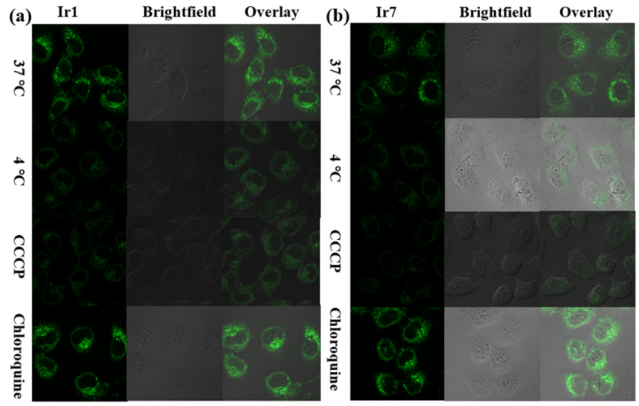

Fig. 2 Effects of temperatures (37 °C or 4 °C), CCCP (50 μM) and chloroquine (50 μM) on cellular uptake of **Ir1** (2 μM) (a) and **Ir7** (2 μM) (b). Scale bar: 20 μm, λ_{ex} = 405 nm, λ_{em} = 430–490 nm.

Ir1 and **Ir7** were investigated using common inhibitors including carbonyl cyanide 3-chloro-phenylhydrazone (CCCP, a metabolic inhibitor) and chloroquine (an endocytosis inhibitor). According to laser confocal microscopy images recorded at λ_{ex} = 405 nm and 37 °C, the punctate green fluorescence in the cytoplasm suggested that **Ir1** and **Ir7** can effectively penetrate into A549 cells after 1 h of incubation (Fig. 2). Small molecule complexes can be transported into cells *via* energy-dependent or energy-independent pathways.[37] When compared to control cells that were incubated at 37 °C, the fluorescence intensity of A549 cells showed a significant decrease when treated with **Ir1** and **Ir7** at a low temperature (4 °C) or pretreated with CCCP (Fig. 2). Thus, these cyclometalated complexes were transported into A549 cells mainly through an energy-dependent pathway. Furthermore, the intracellular fluorescence intensity did not show any difference between A549 cells treated with chloroquine and the untreated group, indicating that endocytosis was not responsible for the uptake pathway of **Ir1** and **Ir7**.

2.7. Cellular localization

Intracellular localization analysis was performed using laser confocal microscopy to evaluate the possible cellular target of these complexes. In this study, three different probes were used to investigate the localization of **Ir1** and **Ir7** in A549 cells (Fig. 3). These probes were specific to the nucleus (DAPI), lysosomes (LTDR) and mitochondria (MTDR), respectively. After treating the cells with the probes and the complexes, it was observed that the complexes effectively penetrated the cells and predominantly localized in the mitochondria. Specifically, the PCC values for DAPI (PCC: 0) and LTDR (PCC: 0.17–0.21) were low (Table 2), indicating that these complexes were not effectively localized in the nucleus and lysosomes. However, the observation of high PCC values (0.81–0.85) for MTDR (Table 2) suggested that these complexes mainly accumulated in the mitochondria and the cytotoxicity of these complexes may be due to mitochondria-mediated cell death.

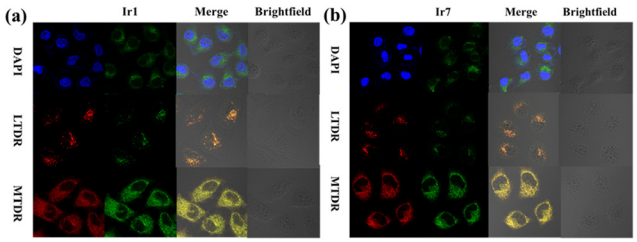

Fig. 3 Determination of Intracellular localization of **Ir1** (a) and **Ir7** (b) by confocal microscopy. A549 cells were incubated with **Ir1** and **Ir7** (2 μM) for 1 h at 3 7 °C and then co-incubated with DAPI (1 μg mL^{-1}), LTDR (75 nM) or MTDR (500 nM) for 1 h, respectively. **Ir1** and **Ir7**, λ_{ex} = 405 nm, λ_{em} = 460–520 nm; DAPI, λ_{ex} = 345 nm, λ_{em} = 410–455 nm; LTDR, λ_{ex} = 594 nm, λ_{em} = 600–660 nm; MTDR, λ_{ex} = 644 nm, λ_{em} = 660–720 nm. Scale bar: 20 μm. The green, red and blue fluorescence represent **Ir1** and **Ir7**, lysosome or mitochondria, and nucleus, respectively.

Table 2 The PCC values for DAPI, LTDR and MTDR

Complexes	DAPI	LTDR	MTDR
Ir1	0	0.21	0.81
Ir7	0	0.17	0.85

Due to the presence of more mitochondria in cancer cells than in normal cells, cancer cells are more sensitive to mitochondrial disruption than normal cells. This may be related to the low anticancer selectivity of these complexes (SI: 1.62–1.98) in this system. It was observed that **Ir1** and **Ir7** have a high positive zeta potential (**Ir1**: 35.62 ± 0.13, **Ir7**: 48.89 ± 0.09) (Fig. S50 and S51†), which can facilitate the complexes to target the mitochondria that had negative charges on their surface once they enter the cytosol. The distribution coefficient (log *P*) values of **Ir1** and **Ir7** were determined using the shake-flask method. These complexes exhibited high lipophilicity, with log *P* values ranging from 1.07 to 1.21 (**Ir1**: 1.21, **Ir7**: 1.07). The similar cytotoxicity of these complexes against cancer cells was also consistent with a slight change in their lipophilicity. Thus, the high lipophilicity of these complexes may also contribute to their ability to target mitochondria. The total cellular accumulation of complexes **Ir1** and **Ir7** was quantified in A549 cells treated with each complex (5 μM) for 48 h by ICP-MS to determine if there was a correlation between cellular uptake levels of the complexes and cytotoxicity. The values of the intracellular metal accumulation in A549 cells for **Ir1** (0.713 ng μg^{-1} protein) and **Ir7** (0.658 ng μg^{-1} protein) were similar, which was also consistent with their slight change in cytotoxicity and log *P*.

2.8. Mitochondrial membrane depolarization

Since these complexes can selectively accumulate in mitochondria, their potential impact on mitochondrial function was also examined. The maintenance of mitochondrial membrane potential (MMP, $\Delta\psi_m$) is crucial for the mitochondrial structure and energy production. A loss of MMP is often an early

indication of the mitochondrion-mediated apoptosis pathway.[38–42] In order to measure the $\Delta\psi_m$, A549 cells were treated with **Ir1** or **Ir7** at concentrations ranging from 0.5 × IC_{50} to 2 × IC_{50}. The changes in MMP were detected through JC-1 staining and flow cytometry. When there was a loss of mitochondrial potential, the ratio of red/green fluorescence intensity decreased. Compared to untreated cells, both **Ir1** and **Ir7** could induce concentration-dependent mitochondrial dysfunction in A549 cells. Specifically, when the concentrations of **Ir1** and **Ir7** were increased from 0.5 × IC_{50} to 2 × IC_{50}, the percentages of mitochondrial membrane depolarization in A549 cells exhibited a significant increase, from 17.78% and 14.35% to 58.21% and 47.19%, respectively (Fig. 4). These results support the speculation that **Ir1** and **Ir7** could exert their anticancer actions by targeting mitochondria and inducing mitochondrial dysfunction.

2.9. Cellular ROS determination

Mitochondria are strongly associated with the production of intracellular reactive oxygen species (ROS).[43–45] Various anticancer drugs can generate excessive levels of ROS and thus lead to oxidative stress and activate cell death processes.[46,47] Previous studies have shown that the generation of reactive oxygen species (ROS) in cells is highly related to mitochondria. Dysfunctional mitochondria cannot effectively regulate ROS production, which results in increased oxidative stress in cancer cells.[48,49] Therefore, we subsequently investigated the impact of these complexes on intracellular ROS levels in both A549 and A549/DPP cells. After staining with DCFH-DA, we measured the total ROS levels induced by **Ir1** and **Ir7** at concentrations of 0.5, 1, and 2 × IC_{50} using fluorescence microscopy (Fig. 5 and S52–S54†). The cells treated with **Ir1** and **Ir7** exhibited a concentration-dependent increase in intracellular ROS levels when compared to the control cells, which suggested that ROS generation was a key factor in causing cell death for these complexes. Notably, the ROS levels in cisplatin-resistant A549/DPP cells treated with **Ir1** also increased in a concentration-dependent manner. Moreover, the level of fluorescence intensity observed in A549/DDP cells, which was directly proportional to the levels of ROS, was found to be comparable to that in A549 cells upon exposure to **Ir1** at the same concentration. This result implied that the ability of these complexes to overcome cisplatin resistance can be attributed to the redox mechanism caused by the overproduction of ROS.

2.10. Apoptosis and cell cycle arrest

Apoptosis is a process of programmed cell death. Many transition metal-based anticancer complexes have been reported to activate apoptosis and inhibit cell growth.[50] The induction of apoptosis is closely related to the disruption of redox balance.

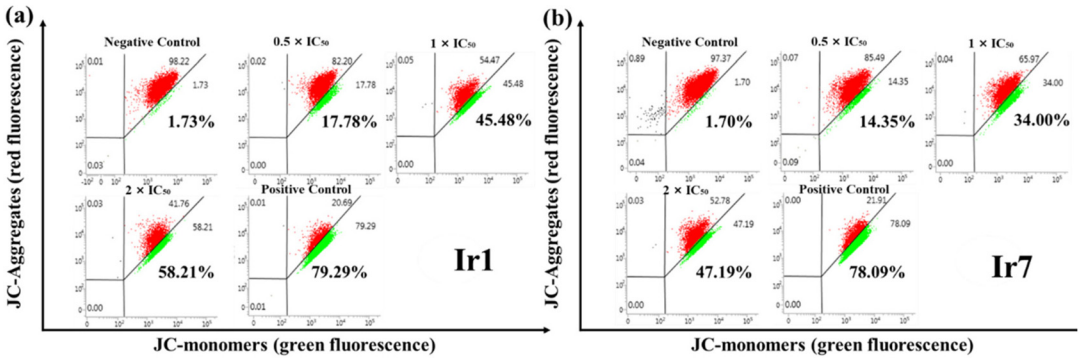

Fig. 4 Changes in mitochondrial membrane potential of A549 cancer cells induced by **Ir1** (a) and **Ir7** (b).

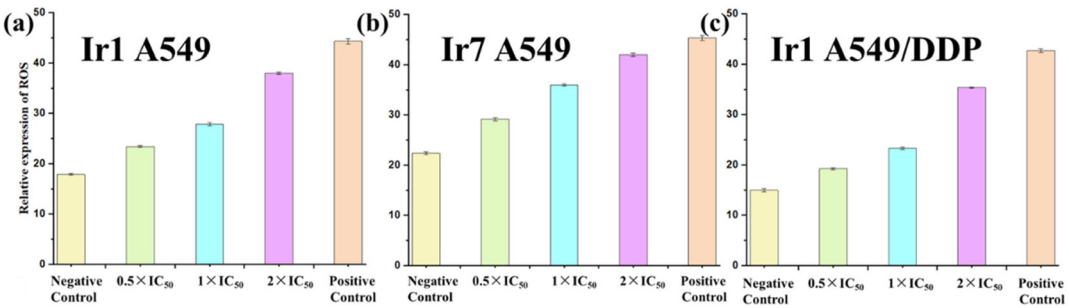

Fig. 5 Analysis of ROS levels using a fluorescence microscope after A549 cells were treated with **Ir1** (a) and **Ir7** (b) for 24 h at 37 °C. Analysis of ROS levels using a fluorescence microscope after A549/DDP cells were treated with **Ir1** (c) for 24 h at 37 °C. Stained with DCFH-DA. Data are quoted as mean ± SD of three replicates. *p*-Values were calculated after a test against the negative control data, $p < 0.05$.

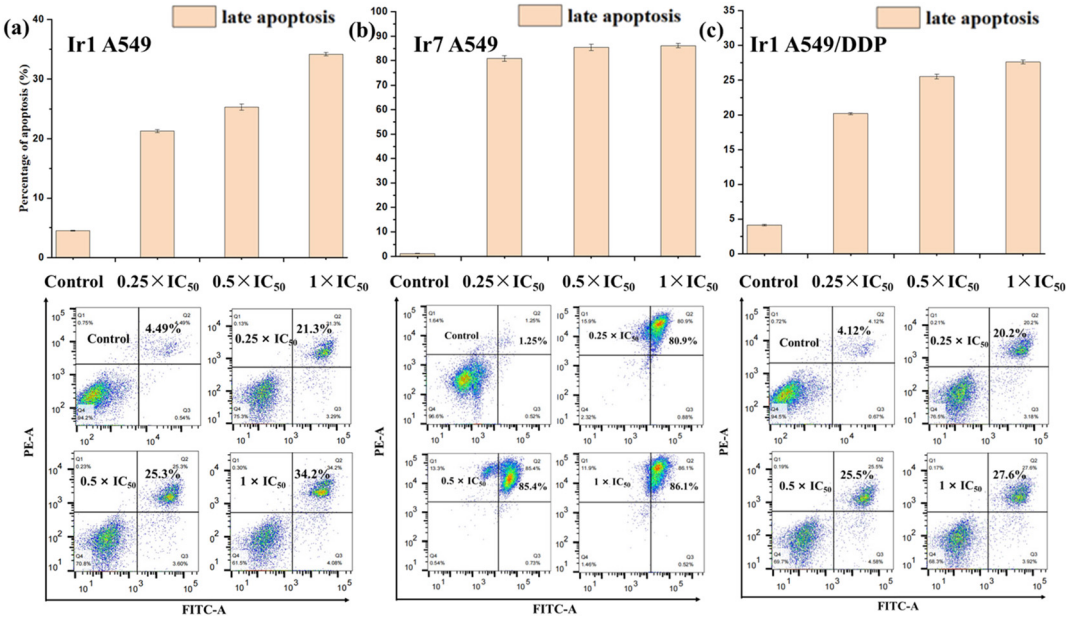

Fig. 6 Apoptosis analysis and the corresponding histograms of apoptosis analysis for A549 cells after 48 h of exposure to **Ir1** (a) and **Ir7** (b) at 37 °C. Apoptosis analysis and the corresponding histograms of apoptosis analysis for A549/DDP cells after 48 h of exposure to **Ir1** (c) at 37 °C. Determined by flow cytometry using annexin V-FITC *vs.* PI staining. Data are quoted as mean ± SD of three replicates. *p*-Values were calculated after a test against the negative control data, $p < 0.05$.

Ir1 and **Ir7** were selected to measure whether they can induce cell apoptosis using the dual-staining annexin V/PI assay. A549 and A549/DPP cells were treated with **Ir1** or **Ir7** at the concentrations of 0.25, 0.5 and 1 × IC_{50} for 48 h and analyzed by flow cytometry (Fig. 6). Compared to the control group, an increase in the percentage of late apoptotic cells was observed for **Ir1** and **Ir7**. In particular, the late apoptotic cell populations increased in an obvious concentration-dependent manner for **Ir1**. When the concentration of **Ir1** and **Ir7** was at 1 × IC_{50}, 34.2% and 86.1% of A549 cells underwent late apoptosis. A similar trend was also observed in the A549/DDP cells treated with **Ir1** (Fig. 6). However, the percentage of A549/DDP cells that underwent late apoptosis was lower than that of A549 cells, with 27.6% of cells undergoing late apoptosis (1 × IC_{50}). These results indicated that the cyclometalated iridium(III) complexes in this system can induce cell death *via* the apoptotic pathway.

Some anticancer complexes have been found to promote apoptosis by arresting the cell cycle.[9,10,51] The cell cycle assay was further performed to measure whether **Ir1** and **Ir7** could induce cell cycle arrest. The effect of **Ir1** and **Ir7** on cell cycle arrest in A549 cells was detected by flow cytometry (Fig. 7 and S55, S56†). When A549 cells were treated with **Ir1** for 24 hours at concentrations of 0.25 and 0.5 × IC_{50}, the proportion of cells in the G_2/M phase increased in a concentration-dependent manner (control: 6.69% *vs.* 0.25 × IC_{50}: 15.10% *vs.* 0.5 × IC_{50}: 19.09%). When A549 cells were treated with **Ir7** at the same duration and concentration, the proportion of cells in the S phase increased in a concentration-dependent manner (control: 29.77% *vs.* 0.25 × IC_{50}: 31.89% *vs.* 0.5 × IC_{50}: 36.08%)

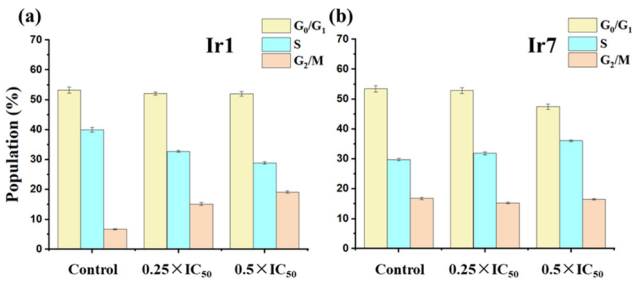

Fig. 7 Flow cytometry data for cell cycle distribution of A549 cancer cells exposed to **Ir1** (a) and **Ir7** (b) for 24 h. The concentrations used were 0.25 × IC_{50} and 0.5 × IC_{50}. Cell staining for flow cytometry was carried out using PI/RNase. Data are quoted as mean ± SD of three replicates. *p*-Values were calculated after a test against the negative control data, $p < 0.05$.

(Fig. 7 and S55, S56†). The different cell cycle perturbation may depend on the activation of various cyclin/Cdk complexes by compounds.[37]

2.11. Lysosomal damage

Lysosomes are organelles surrounded by membranes that play a crucial role in many physiological processes.[52–54] To assess whether cell death was due to lysosomal damage, we used acridine orange as a probe to evaluate lysosomal dysfunction. Acridine orange is the most commonly used and commercially available LysoTracker that emits red fluorescence in lysosomes and green fluorescence in cytosol and nuclei.[55,56] When only A549 cells were treated with acridine orange (5 μM), red fluo-

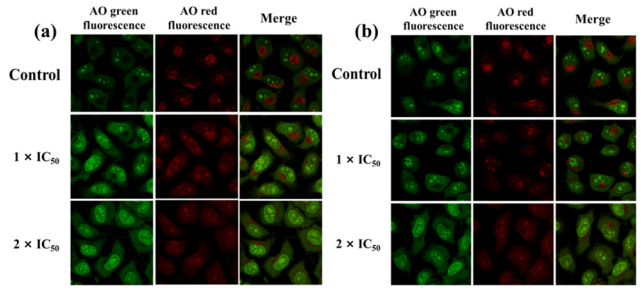

Fig. 8 Confocal luminescence imaging of acridine orange (5 μM) stained A549 cells exposed to **Ir1** (a) and **Ir7** (b). Concentrations used were 1 × IC_{50} and 2 × IC_{50}. λ_{ex}: 488 nm; λ_{em}: 490–530 nm (green channel); 605–645 nm (red channel).

rescence was observed in the lysosomes, indicating that the lysosomes of A549 cells were intact. The treatment with complexes **Ir1** and **Ir7** at the concentrations of 1 × IC_{50} and 2 × IC_{50} only led to a slight change of AO red fluorescence compared to the control, thereby indicating that the lysosomal integrity of A549 cells was not disrupted under such conditions (Fig. 8). This result was also consistent with the aforementioned low accumulation efficiency of these complexes in lysosomes (section 2.7).

2.12. Inhibition of cell migration

Preventing the spread of cancer cells is difficult for cancer treatment. When the surface adhesion of malignant cells decreases, they can move away from the original tumor site and travel to other organs.[57,58] To assess the inhibitory effect of **Ir1** and **Ir7** on the migration of A549 cancer cells, a wound-healing assay was conducted (Fig. 9). Compared to the control group (42.89% and 38.38%), the wound closure rate (WCR) of A549 cancer cells treated with **Ir1** and **Ir7** decreased to 13.49% and 18.17%, respectively, at 0.5 × IC_{50} and presented a concentration-dependent characteristic. These results suggest that these cyclometalated complexes can impede the *in vitro* migration of A549 cancer cells.

3. Conclusions

In conclusion, we synthesized a series of neutral and cationic amine–imine cyclometalated iridium(III) complexes. These complexes were stable in aqueous media. The moderate fluorescence and the affinity towards BSA for these complexes were also verified by spectroscopic studies. **Ir1–Ir12** showed promising cytotoxicity against lung cancer A549 cells, cervical carcinoma HeLa cells, and human liver carcinoma HepG2 cells. In particular, the high cytotoxicity against cisplatin-resistant A549/DDP cells was also observed for these complexes, suggesting that they were not cross-resistant with cisplatin. The charge pattern of the metal center (neutral or cationic) and ligand substituents showed little influence on the cytotoxicity and selectivity of these complexes. The typical complexes **Ir1** and **Ir7** were observed to enter the cells of A549 through an energy-dependent pathway. These complexes can target mitochondria, lead to depolarization of the mitochon-

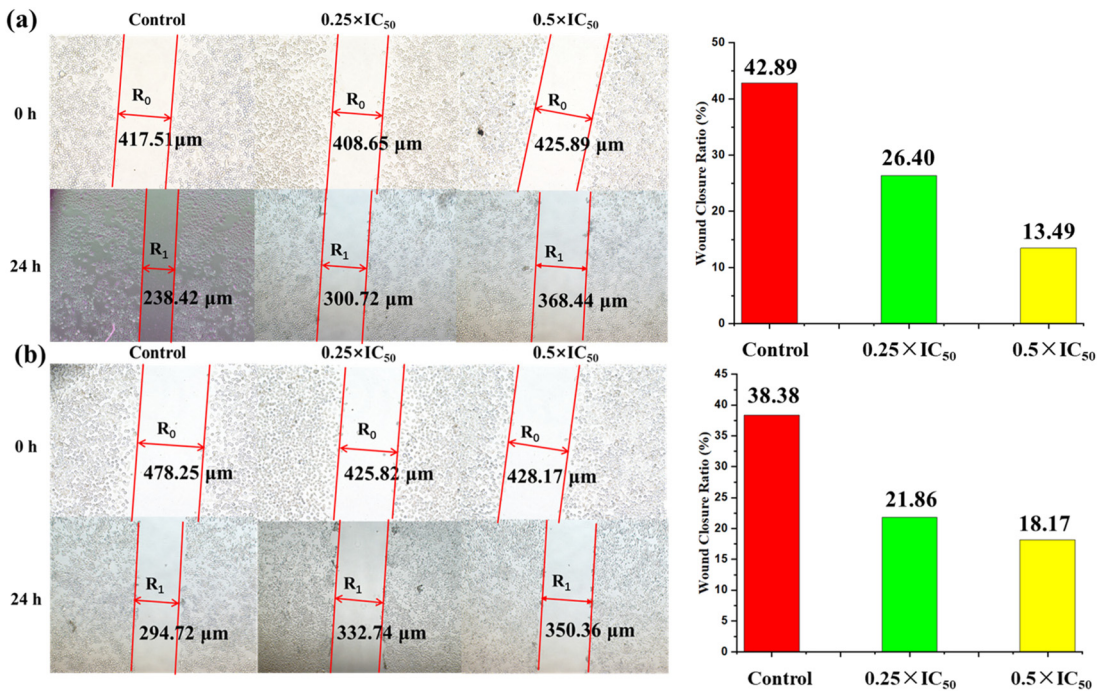

Fig. 9 (a) Wound-healing assay and histogram analysis for A549 cells treated with **Ir1** for 24 h. (b) Wound-healing assay and histogram analysis for A549 cells treated with **Ir7** for 24 h. Typical images were taken at 0 h and 24 h. The widths of the wounds are indicated with the lines (μm). Scale bar: 100 μm. Wound closure rate = $(R_0 - R_1)/R_0 \times 100\%$.

drial membrane, and trigger the overproduction of intracellular ROS. **Ir1** and **Ir7** could induce late cell apoptosis and disrupt the cell cycle in the G_2/M or S phase. The migration ability of A549 cells was also inhibited by these complexes. These types of neutral and cationic cyclometalated amine–imine complexes may serve as a potent platform for developing redox-based anticancer agents.

4. Experimental section

4.1. General considerations

The chemicals and reagents used in the study were purchased from commercial suppliers and were of analytical grade. Human cells (A549 cells, A549/DDP cells, HeLa cells, HepG2 cells and BESA-2B cells) were obtained from the Shanghai Institute of Biochemistry and Cell Biology. BSA was obtained from Energy Chemical Company. Cell culture media were purchased from Solebo Technology Limited company. The ligands **L1–L3** and the bimetallic precursors **D1–D5** were prepared using literature methods.[9,25,26,33,34] The ^{1}H, ^{13}C{^{1}H} NMR and ^{31}P{^{1}H} NMR spectra were obtained in 5 mm NMR tubes at 25 °C unless otherwise stated on Bruker DPX 500 spectrometers. The ^{1}H NMR chemical shifts were internally referenced to TMS (0 ppm) or solvents. All data processing was carried out using XWIN-NMR version 3.6 (Bruker UK Ltd). The TU-1901 UV-visible recording spectrophotometer was used to determine absorption spectroscopy. The Thermo LTQ Orbitrap XL spectrometer was used to record the MS of the novel compounds. The Vario El cube was used to perform elemental analysis (C, H, N). A detailed description of biological experiments is also shown in the ESI.†

4.2. Synthesis of complexes

4.2.1. Synthesis of neutral iridium(III) complexes. A CH_2Cl_2/CH_3OH (v/v, *ca.* 1 : 1) mixture solution of bimetallic metal precursors (1 eq.), ligands (2 eq.) and a slight excess of the deprotonating agent NaOAc (5 eq.) were stirred at room temperature for 6 h. The solvents were removed using a rotoevaporator. The solid was dissolved in CH_2Cl_2 and filtered. Upon removal of the solvent, the residue was recrystallized from CH_2Cl_2 and *n*-hexane to yield a pale red powder.

Ir1: yield 69 mg (57%). ^{1}H NMR (500 MHz, $CDCl_3$) δ 8.98 (m, 2H), 8.06 (s, 1H, C*H*═N), 7.87 (d, 1H), 7.84 (m, 1H), 7.74 (m, 1H), 7.65 (m, 1H), 7.58 (d, 1H), 7.54 (m, 1H), 7.08 (d, 2H), 7.02 (m, 2H), 6.87 (m, 2H), 6.66 (m, 4H), 6.51 (m, 1H), 6.29 (m, 2H), 6.11 (m, 1H), 6.03 (m, 2H), 1.13 (s, 9H, C(CH_3)$_3$). ^{13}C NMR (126 MHz, DMSO-d_6) δ 168.96 (*C*H═N), 151.82, 150.71, 149.00, 144.78, 139.37, 137.17, 136.76, 135.97, 132.46, 131.80, 131.05, 128.46, 127.89, 123.71, 123.44, 123.31, 122.73, 122.31, 122.05, 121.81, 119.09, 118.45, 109.47, 33.57 (*C*(CH$_3$)$_3$), 31.08 (C(*C*H$_3$)$_3$), 24.77 (C(*C*H$_3$)$_3$). ESI-MS (*m*/*z*): calcd for $C_{39}H_{36}IrN_4$ 753.25692, found 753.25407, [M + H]$^+$. Elemental analysis: calcd for $C_{39}H_{35}IrN_4$: C, 62.29; H, 4.69; N, 7.45, found: C, 62.52; H, 4.41; N, 7.12.

Ir2: yield 65 mg (55%). ^{1}H NMR (500 MHz, $CDCl_3$) δ 8.83 (m, 2H), 8.04 (s, 1H, C*H*═N), 7.72 (d, 1H), 7.63 (t, 1H), 7.57 (d, 1H), 7.51 (d, 1H), 7.38 (d, 1H), 7.01 (m, 5H), 6.69 (d, 2H), 6.43 (m, 1H), 6.26 (d, 1H), 6.10 (m, 1H), 6.04 (d, 2H), 5.93 (t, 1H), 5.84 (d, 1H), 5.68 (t, 1H), 3.51 (d, 6H, OCH_3), 1.14 (s, 9H, C(CH_3)$_3$). ^{13}C NMR (126 MHz, $CDCl_3$) δ 167.69 (*C*H═N), 160.04, 159.83, 149.65, 149.17, 147.19, 137.68, 136.33, 136.14, 134.60, 131.74, 128.58, 128.23, 127.65, 126.01, 125.17, 124.90, 123.94, 122.58, 121.91, 120.61, 120.50, 119.22, 118.61, 117.94, 117.52, 117.22, 116.96, 114.16, 106.94, 105.54, 65.66 (O*C*H$_3$), 54.53 (O*C*H$_3$), 34.05 (*C*(CH$_3$)$_3$), 31.34 (C(*C*H$_3$)$_3$), 29.72 (C(*C*H$_3$)$_3$). ESI-MS (*m*/*z*): calcd for $C_{41}H_{40}IrN_4O_2$ 813.27805, found 813.27562, [M + H]$^+$. Elemental analysis: calcd for $C_{41}H_{39}IrN_4O_2$: C, 60.65; H, 4.84; N, 6.90, found: C, 60.98; H, 4.52; N, 6.54.

Ir3: yield 58 mg (52%). ^{1}H NMR (500 MHz, $CDCl_3$) δ 8.87 (m, 2H), 8.04 (s, 1H, C*H*═N), 7.81 (d, 1H), 7.67 (t, 1H), 7.60 (t, 1H), 7.49 (m, 2H), 7.03 (m, 2H), 6.98 (m, 3H), 6.65 (d, 3H), 6.28 (m, 2H), 6.11 (s, 1H), 6.00 (d, 2H), 5.93 (d, 2H), 2.04 (s, 3H, CH_3), 1.95 (s, 3H, CH_3), 1.14 (s, 9H, C(CH_3)$_3$). ^{13}C NMR (126 MHz, $CDCl_3$) δ 169.76 (*C*H═N), 168.25, 160.64, 157.22, 153.78, 152.30, 150.63, 149.12, 148.91, 146.46, 142.17, 142.06, 138.76, 138.07, 135.98, 135.69, 134.21, 133.34, 130.99, 123.66, 123.34, 123.16, 122.81, 122.51, 121.84, 121.41, 120.88, 120.55, 118.28, 117.48, 115.84, 109.58, 33.93 (*C*(CH$_3$)$_3$), 31.33 (C(*C*H$_3$)$_3$), 21.66 (*C*H$_3$), 21.61 (*C*H$_3$). ESI-MS (*m*/*z*): calcd for $C_{41}H_{40}IrN_4$ 781.28822, found 781.28875, [M + H]$^+$. Elemental analysis: calcd for $C_{41}H_{39}IrN_4$: C, 63.13; H, 5.04; N, 7.18, found: C, 63.48; H, 4.71; N, 6.83.

Ir4: yield 55 mg (53%). ^{1}H NMR (500 MHz, $CDCl_3$) δ 8.88 (m, 2H), 8.28 (d, 1H), 8.03 (s, 1H, C*H*═N), 7.92 (d, 1H), 7.77 (t, 1H), 7.71 (t, 1H), 7.14 (m, 2H), 7.00 (m, 2H), 6.75 (d, 2H), 6.36 (t, 1H), 6.31 (d, 1H), 6.05 (m, 4H), 5.73 (m, 1H), 5.57 (m, 1H), 1.17 (s, 9H, C(CH_3)$_3$). ^{13}C NMR (126 MHz, $CDCl_3$) δ 166.31 (*C*H═N), 164.95, 157.76, 152.21, 150.19, 149.28, 149.15, 147.52, 137.16, 136.94, 135.77, 131.78, 123.99, 122.85, 122.59, 122.36, 122.20, 121.43, 115.39, 114.73, 114.39, 110.45, 97.17, 31.25 (*C*(CH$_3$)$_3$), 14.12 (C(*C*H$_3$)$_3$). ESI-MS (*m*/*z*): calcd for $C_{39}H_{32}F_4IrN_4$ 825.21923, found 825.22379, [M + H]$^+$. Elemental analysis: calcd for $C_{39}H_{31}F_4IrN_4$: C, 56.85; H, 3.79; N, 6.80, found: C, 57.14; H, 3.56; N, 6.49.

Ir5: yield 64 mg (53%). ^{1}H NMR (500 MHz, $CDCl_3$) δ 8.93 (m, 2H), 8.06 (s, 1H, C*H*═N), 7.95 (d, 1H), 7.85 (m, 1H), 7.78 (m, 1H), 7.63 (m, 2H), 7.22 (d, 3H), 7.09 (m, 3H), 6.98 (d, 2H), 6.75 (d, 1H), 6.66 (d, 2H), 6.46 (s, 1H), 6.30 (d, 1H), 5.96 (s, 2H), 1.11 (s, 9H, C(CH_3)$_3$). ^{13}C NMR (126 MHz, $CDCl_3$) δ 168.19 (*C*H═N), 157.74, 152.17, 150.29, 149.48, 149.33, 148.27, 136.96, 136.66, 135.82, 128.28, 124.12, 123.37, 123.27, 122.85, 122.62, 122.45, 119.72, 118.89, 118.05, 116.94, 33.95 (*C*(CH$_3$)$_3$), 31.23 (C(*C*H$_3$)$_3$). ESI-MS (*m*/*z*): calcd for $C_{41}H_{34}F_6IrN_4$ 889.23169, found 889.22894, [M + H]$^+$. Elemental analysis: calcd for $C_{41}H_{33}F_4IrN_4$: C, 55.46; H, 3.75; N, 6.31, found: C, 55.84; H, 3.54; N, 6.11.

Ir6: yield 59 mg (55%). ^{1}H NMR (500 MHz, $CDCl_3$) δ 8.89 (m, 2H), 8.00 (s, 1H, C*H*═N), 7.86 (d, 1H), 7.68 (t, 1H), 7.62 (t, 1H), 7.57 (d, 1H), 7.52 (d, 1H), 7.07 (d, 3H), 6.97 (d, 1H), 6.95

(m, 1H), 6.84 (t, 1H), 6.69 (t, 1H), 6.57 (m, 2H), 6.46 (d, 2H), 6.30 (d, 1H), 6.26 (d, 1H), 6.15 (d, 1H), 6.02 (d, 2H), 5.94 (t, 1H), 2.08 (s, 3H, CH_3). ^{13}C NMR (126 MHz, $CDCl_3$) δ 168.21 (*C*H═N), 157.63, 152.32, 151.44, 149.31, 149.07, 144.72, 144.53, 136.14, 135.87, 133.17, 132.48, 131.17, 128.99, 128.76, 127.57, 123.52, 123.34, 122.86, 122.00, 121.12, 120.70, 119.52, 118.71, 117.92, 115.87, 109.74, 31.62 (*C*(CH_3)$_3$), 22.69 (C(*C*H_3)$_3$), 20.68 (C(*C*H_3)$_3$), 14.15 (*C*H_3). ESI-MS (*m*/*z*): calcd for $C_{36}H_{30}IrN_4$ 711.20997, found 711.20743, $[M + H]^+$. Elemental analysis: calcd for $C_{36}H_{29}IrN_4$: C, 60.91; H, 4.12; N, 7.89, found: C, 61.25; H, 3.77; N, 7.68.

4.2.2. Synthesis of cationic iridium(III) complexes. A CH_2Cl_2/CH_3OH (v/v, *ca.* 1 : 1) mixture solution of bimetallic metal precursors (1 eq.), ligands (2 eq.) and NH_4PF_6 (5 eq.) was stirred at room temperature for 6 h. The solvents were removed using a rotoevaporator. The solid was dissolved in CH_2Cl_2 and filtered. Upon removal of the solvent, the residue was recrystallized from CH_2Cl_2 and *n*-hexane to yield a pale yellow powder.

Ir7: yield 61 mg (54%). ^{1}H NMR (500 MHz, $CDCl_3$) δ 8.72 (d, 1H), 8.18 (s, 1H, C*H*═N), 8.00 (d, 1H), 7.87 (m, 1H), 7.77 (d, 1H), 7.67 (m, 3H), 7.39 (m, 2H), 7.15 (m, 2H), 7.08 (d, 1H), 6.92 (t, 1H), 6.80 (m, 2H), 6.69 (d, 2H), 6.63 (t, 1H), 6.47 (d, 1H), 6.42 (d, 1H), 6.20 (d, 1H), 6.08 (d, 1H), 6.02 (d, 2H), 1.17 (s, 9H, C(CH_3)$_3$). ^{13}C NMR (126 MHz, $CDCl_3$) δ 167.48 (*C*H═N), 167.18, 166.22, 149.75, 149.28, 149.01, 148.65, 146.28, 146.12, 143.93, 139.37, 137.77, 137.73, 133.70, 133.49, 132.72, 131.23, 130.07, 129.32, 128.10, 126.23, 124.58, 124.50, 124.03, 123.28, 122.99, 122.01, 121.73, 121.44, 120.29, 118.91, 118.46, 34.18 (*C*(CH_3)$_3$), 31.28 (C(*C*H_3)$_3$). ^{31}P NMR (202 MHz, $CDCl_3$) δ −144.27 (septet, *J* = 712 Hz, *P*F_6). ESI-MS (*m*/*z*): calcd for $C_{39}H_{36}IrN_4$ 753.25692, found 753.25582, $[M - PF_6]^+$. Elemental analysis: calcd for $C_{39}H_{36}IrN_4PF_6$: C, 52.17; H, 4.04; N, 6.24, found: C, 52.58; H, 3.86; N, 6.10.

Ir8: yield 55 mg (56%). ^{1}H NMR (500 MHz, $CDCl_3$) δ 8.67 (s, 1H), 8.23 (s, 1H, C*H*═N), 7.93 (d, 1H), 7.61 (d, 1H), 7.53 (d, 1H), 7.45 (m, 2H), 7.23 (s, 1H), 7.16 (d, 2H), 7.04 (d, 2H), 6.73 (d, 2H), 6.63 (t, 2H), 6.52 (m, 1H), 6.45 (s, 1H), 6.36 (m, 1H), 6.11 (d, 2H), 5.71 (d, 1H), 5.61 (d, 1H), 3.54 (s, 3H, OCH_3), 3.51 (s, 3H, OCH_3), 1.18 (s, 9H, C(CH_3)$_3$). ^{13}C NMR (126 MHz, $CDCl_3$) δ 167.22 (*C*H═N), 166.16, 160.39, 159.97, 149.44, 149.10, 148.90, 139.71, 137.63, 136.88, 133.66, 132.57, 128.21, 126.03, 125.95, 125.53, 124.56, 124.53, 121.74, 121.62, 120.83, 120.26, 118.09, 117.75, 116.68, 108.61, 106.99, 54.79 (O*C*H_3), 54.66 (O*C*H_3), 34.19 (*C*(CH_3)$_3$), 31.30 (C(*C*H_3)$_3$). ^{31}P NMR (202 MHz, $CDCl_3$) δ −144.44 (septet, *J* = 711 Hz, *P*F_6). ESI-MS (*m*/*z*): calcd for $C_{41}H_{40}IrN_4O_2$ 813.27805, found 813.27531, $[M - PF_6]^+$. Elemental analysis: calcd for $C_{41}H_{40}IrN_4O_2PF_6$: C, 51.41; H, 4.21; N, 5.85, found: C, 51.74; H, 4.03; N, 5.56.

Ir9: yield 62 mg (54%). ^{1}H NMR (500 MHz, $CDCl_3$) δ 8.77 (s, 1H), 8.17 (s, 1H, C*H*═N), 8.02 (d, 1H), 7.93 (m, 1H), 7.77 (d, 1H), 7.69 (d, 1H), 7.65 (m, 2H), 7.48 (m, 2H), 7.31 (s, 1H), 7.15 (t, 2H), 6.98 (m, 2H), 6.79 (m, 3H), 6.72 (d, 1H), 6.65 (d, 1H), 6.52 (d, 2H), 6.19 (d, 1H), 6.09 (d, 1H), 6.04 (s, 1H), 2.15 (s, 3H, CH_3). ^{13}C NMR (126 MHz, $CDCl_3$) δ 166.59 (*C*H═N), 149.77, 137.96, 135.74, 133.67, 133.40, 132.82, 131.20, 129.37, 128.20, 126.19, 122.98, 121.48, 120.68, 118.93, 20.82 (*C*H_3). ^{31}P NMR (202 MHz, $CDCl_3$) δ −144.29 (septet, *J* = 713 Hz, *P*F_6). ESI-MS (*m*/*z*): calcd for $C_{36}H_{30}IrN_4$ 711.20997, found 711.20713, $[M - PF_6]^+$. Elemental analysis: calcd for $C_{36}H_{30}IrN_4PF_6$: C, 50.52; H, 3.53; N, 6.55, found: C, 50.89; H, 3.28; N, 6.31.

Ir10: yield 57 mg (53%). ^{1}H NMR (500 MHz, $CDCl_3$) δ 8.63 (s, 1H), 8.15 (s, 1H, C*H*═N), 7.93 (d, 2H), 7.80 (m, 2H), 7.61 (t, 3H), 7.41 (d, 2H), 7.13 (m, 4H), 6.62 (m, 3H), 6.53 (d, 3H), 6.35 (s, 1H), 6.10 (d, 1H), 5.69 (d, 1H), 5.61 (d, 1H), 3.52 (d, 6H, OCH_3), 2.14 (s, 3H, CH_3). ^{13}C NMR (126 MHz, $CDCl_3$) δ 166.58 (*C*H═N), 160.45, 159.96, 149.56, 149.47, 148.97, 147.15, 144.02, 137.65, 137.25, 135.77, 133.72, 132.83, 128.28, 126.21, 126.00, 125.67, 121.93, 120.77, 120.71, 118.14, 117.95, 116.32, 108.88, 107.56, 106.88, 54.75 (O*C*H_3), 54.65 (O*C*H_3), 20.82 (*C*H_3). ^{31}P NMR (202 MHz, $CDCl_3$) δ −144.44 (septet, *J* = 711 Hz, *P*F_6). ESI-MS (*m*/*z*): calcd for $C_{38}H_{34}IrN_4O_2$ 771.23110, found 771.22917, $[M - PF_6]^+$. Elemental analysis: calcd for $C_{38}H_{34}IrN_4O_2PF_6$: C, 49.83; H, 3.74; N, 6.12, found: C, 50.25; H, 3.54; N, 5.87.

Ir11: yield 56 mg (55%). ^{1}H NMR (500 MHz, $CDCl_3$) δ 8.76 (d, 1H), 8.20 (s, 1H, C*H*═N), 8.01 (d, 1H), 7.97 (m, 1H), 7.77 (d, 1H), 7.69 (t, 1H), 7.65 (m, 2H), 7.47 (d, 1H), 7.42 (d, 1H), 7.29 (s, 1H), 7.21 (d, 1H), 7.15 (d, 1H), 6.94 (t, 1H), 6.79 (m, 2H), 6.72 (t, 1H), 6.65 (t, 1H), 6.57 (m, 1H), 6.44 (d, 1H), 6.25 (d, 2H), 6.19 (d, 1H), 6.11 (t, 2H), 3.65 (s, 3H, OCH_3). ^{13}C NMR (126 MHz, $CDCl_3$) δ 167.54 (*C*H═N), 167.13, 166.70, 157.67, 149.81, 149.20, 148.72, 146.11, 144.01, 142.78, 139.37, 137.89, 137.76, 133.44, 132.78, 130.03, 129.37, 128.20, 126.18, 124.48, 124.28, 123.00, 122.21, 122.05, 121.58, 118.90, 118.68, 112.91, 55.50 (O*C*H_3). ^{31}P NMR (202 MHz, $CDCl_3$) δ −144.25 (septet, *J* = 713 Hz, *P*F_6). ESI-MS (*m*/*z*): calcd for $C_{36}H_{30}IrN_4O$ 727.20434, found 727.20152, $[M - PF_6]^+$. Elemental analysis: calcd for $C_{36}H_{30}IrN_4OPF_6$: C, 49.60; H, 3.47; N, 6.43, found: C, 49.89; H, 3.31; N, 6.19.

Ir12: yield 62 mg (54%). ^{1}H NMR (500 MHz, $CDCl_3$) δ 8.74 (d, 1H), 8.32 (s, 1H, C*H*═N), 7.95 (d, 1H), 7.85 (m, 2H), 7.66 (m, 2H), 7.56 (m, 2H), 7.44 (d, 1H), 7.34 (d, 1H), 7.16 (m, 2H), 6.63 (s, 1H), 6.51 (d, 2H), 6.39 (d, 1H), 6.30 (d, 2H), 6.23 (d, 2H), 5.71 (d, 1H), 5.65 (d, 1H), 3.65 (s, 3H, OCH_3), 3.53 (s, 3H, OCH_3), 3.52 (s, 3H, OCH_3). ^{13}C NMR (126 MHz, $CDCl_3$) δ 166.85 (*C*H═N), 166.65, 160.45, 159.96, 149.50, 149.01, 137.60, 132.79, 125.98, 122.13, 121.97, 118.11, 112.95, 55.50 (O*C*H_3), 54.71 (O*C*H_3), 54.67 (O*C*H_3). ^{31}P NMR (202 MHz, $CDCl_3$) δ −144.19 (septet, *J* = 713 Hz, *P*F_6). ESI-MS (*m*/*z*): calcd for $C_{38}H_{34}IrN_4O_3$ 787.22546, found 787.22371, $[M - PF_6]^+$. Elemental analysis: calcd for $C_{38}H_{34}IrN_4O_3PF_6$: C, 48.98; H, 3.68; N, 6.01, found: C, 49.24; H, 3.38; N, 5.77.

Conflicts of interest

The authors declare no competing financial interest.

Acknowledgements

We thank the Natural Science Foundation of Shandong Province (ZR2022MB038), the Young Talents Invitation

Program of Shandong Provincial Colleges and Universities, and the Taishan Scholars Program for support and Shiyanjia Lab (https://www.shiyanjia.com) for the mass spectrum test.

References

1 I. Ott and R. Gust, *Arch. Pharm.*, 2007, **340**, 117–126.
2 M. Bashir, I. A. Mantoo, F. Arjmand, S. Tabassum and I. Yousuf, *Coord. Chem. Rev.*, 2023, **487**, 215169.
3 T. S. Prathima, B. Choudhury, M. G. Ahmad, K. Chanda and M. M. Balamurali, *Coord. Chem. Rev.*, 2023, **490**, 215231.
4 A. Zamora, G. Vigueras, V. Rodríguez, M. D. Santana and J. Ruiz, *Coord. Chem. Rev.*, 2018, **360**, 34–76.
5 K. Qiu, Y. Liu, H. Huang, C. Liu, H. Zhu, Y. Chen, L. Ji and H. Chao, *Dalton Trans.*, 2016, **45**, 16144–16147.
6 Y. Yang, L. Guo, X. Ge, W. Chen, H. Zhou, T. Zhu, X. Li, S. Tuo and Z. Liu, *Dyes Pigm.*, 2020, **176**, 108220.
7 G. Miklossy, T. S. Hilliard and J. Turkson, *Nat. Rev. Drug Discovery*, 2013, **12**, 611–629.
8 C.-H. Leung, H.-J. Zhong, H. Yang, Z. Cheng, D. S.-H. Chan, V. P.-Y. Ma, R. Abagyan, C.-Y. Wong and D.-L. Ma, *Angew. Chem., Int. Ed.*, 2012, **51**, 9010–9014.
9 Q. Du, L. Zhao, L. Guo, X. Ge, S. Zhang, Z. Xu and Z. Liu, *Appl. Organomet. Chem.*, 2018, **33**, e4746.
10 Z. Tian, Y. Yang, L. Guo, G. Zhong, J. Li and Z. Liu, *Inorg. Chem. Front.*, 2018, **5**, 3106–3112.
11 C. C. Konkankit, S. C. Marker, K. M. Knopf and J. J. Wilson, *Dalton Trans.*, 2018, **47**, 9934–9974.
12 L. Zeng, P. Gupta, Y. Chen, E. Wang, L. Ji, H. Chao and Z.-S. Chen, *Chem. Soc. Rev.*, 2017, **46**, 5771–5804.
13 K. Henze and W. Martin, *Nature*, 2003, **426**, 127–128.
14 R. J. Youle and D. P. Narendra, *Nat. Rev. Mol. Cell Biol.*, 2011, **12**, 9–14.
15 H. M. McBride, M. Neuspiel and S. Wasiak, *Curr. Biol.*, 2006, **16**, R551–R560.
16 Y. Chen, L. Qiao, L. Ji and H. Chao, *Biomaterials*, 2014, **35**, 2–13.
17 X. Chen, L. Sun, Y. Chen, X. Cheng, W. Wu, L. Ji and H. Chao, *Biomaterials*, 2015, **58**, 72–81.
18 Y. Chen, L. Qiao, B. Yu, G. Li, C. Liu, L. Ji and H. Chao, *Chem. Commun.*, 2013, **49**, 11095–11097.
19 C. Jin, J. Liu, Y. Chen, L. Zeng, R. Guan, C. Ouyang, L. Ji and H. Chao, *Chem. – Eur. J.*, 2015, **21**, 12000–12010.
20 R.-R. Ye, C.-P. Tan, L.-N. Ji and Z.-W. Mao, *Dalton Trans.*, 2016, **45**, 13042–13051.
21 F.-X. Wang, M.-H. Chen, X.-Y. Hu, R.-R. Ye, C.-P. Tan, L.-N. Ji and Z.-W. Mao, *Sci. Rep.*, 2016, **6**, 38954.
22 J.-J. Cao, C.-P. Tan, M.-H. Chen, N. Wu, D.-Y. Yao, X.-G. Liu, L.-N. Ji and Z.-W. Mao, *Chem. Sci.*, 2017, **8**, 631–640.
23 M.-H. Chen, F.-X. Wang, J.-J. Cao, C.-P. Tan, L.-N. Ji and Z.-W. Mao, *ACS Appl. Mater. Interfaces*, 2017, **9**, 13304–13314.
24 M. Ouyang, L. Zeng, H. Huang, C. Jin, J. Liu, Y. Chen, L. Ji and H. Chao, *Dalton Trans.*, 2017, **46**, 6734–6744.
25 X. D. Song, X. Kong, S. F. He, J. X. Chen, J. Sun, B. B. Chen, J. W. Zhao and Z. W. Mao, *Eur. J. Med. Chem.*, 2017, **138**, 246–254.
26 K. Xiong, Y. Chen, C. Ouyang, R. L. Guan, L. N. Ji and H. Chao, *Biochimie*, 2016, **125**, 186–194.
27 Z. Nadova, L. Lenkavska, A. Fragola, S. Bonneau, F. Sureau and P. Miskovsky, *Biophys. J.*, 2016, **110**, 470a.
28 M. P. Murphy, *Biochim. Biophys. Acta, Bioenerg.*, 1989, **977**, 123–141.
29 S. Trapp and R. W. Horobin, *Eur. Biophys. J.*, 2005, **34**, 959–966.
30 S. G. Rubio, N. M. Pastor, C. Garcia, V. G. Almendro-Vedia, I. Ferrer, P. Natale, L. Paz-Ares, M. P. Lillo and I. López-Montero, *Front. Oncol.*, 2018, **8**, 514.
31 K. Qiu, Y. Chen, T. W. Rees, L. Ji and H. Chao, *Coord. Chem. Rev.*, 2019, **378**, 66–86.
32 S. P. Li, T. S. Tang, K. S. Yiu and K. K. Lo, *Chem. – Eur. J.*, 2012, **18**, 13342–13354.
33 P. Brüggemann, K. Mzyk, M. Molter, J. Nellesen, K. Schaper and C. Ganter, *Eur. J. Inorg. Chem.*, 2021, e202100894.
34 B. Rigo, P. Gautret, R. Akue-Gedu and J.-P. Lelieur, *Synthesis*, 2007, 3319–3322.
35 Y. Yang, L. Guo, X. Ge, Z. Tian, Y. Gong, H. Zheng, Q. Du, X. Zheng and Z. Liu, *Dyes Pigm.*, 2019, **161**, 119–129.
36 H. Xiang, H. Chen, H. P. Tham, S. Z. F. Phua, J. G. Liu and Y. Zhao, *ACS Appl. Mater. Interfaces*, 2017, **9**, 27553–27562.
37 B. Schutte, L. Nieland, M. van Engeland, M. E. R. Henfling, L. Meijer and F. C. S. Ramaekers, *Exp. Cell Res.*, 1997, **236**, 4–15.
38 R. L. Panchangam, R. N. Rao, M. M. Balamurali, T. B. Hingamire, D. Shanmugam, V. Manickam and K. Chanda, *Inorg. Chem.*, 2021, **60**, 17593–17607.
39 I. Romero-Canelon, M. Mos and P. J. Sadler, *J. Med. Chem.*, 2015, **58**, 7874–7880.
40 A. C. Carrasco, V. Rodriguez-Fanjul, A. Habtemariam and A. M. Pizarro, *J. Med. Chem.*, 2020, **63**, 4005–4021.
41 A. Arunachalam, R. Rengan, D. Umapathy and A. J. V. Arockiam, *Organometallics*, 2022, **41**, 2474–2486.
42 I. Echevarria, E. Zafon, S. Barrabes, M. A. Martinez, S. Ramos-Gomez, N. Ortega, B. R. Manzano, F. A. Jalon, R. Quesada, G. Espino and A. Massaguer, *J. Inorg. Biochem.*, 2022, **231**, 111790.
43 J. D. Dunn, L. A. Alvarez, X. Zhang and T. Soldati, *Redox Biol.*, 2015, **6**, 472–485.
44 D. Trachootham, J. Alexandre and P. Huang, *Nat. Rev. Drug Discovery*, 2009, **8**, 579–591.
45 D. B. Zorov, M. Juhaszova and S. J. Sollott, *Physiol. Rev.*, 2014, **94**, 909–950.
46 H. U. Simon, A. Haj-Yehia and F. Levi-Schaffer, *Apoptosis*, 2000, **5**, 415–418.
47 Z. Liu, I. Romero-Canelón, B. Qamar, J. M. Hearn, A. Habtemariam, N. P. E. Barry, A. M. Pizarro, G. J. Clarkson and P. J. Sadler, *Angew. Chem., Int. Ed.*, 2014, **53**, 3941–3946.
48 I. E. Scheffler, *Mitochondrion*, 2001, **1**, 3–31.
49 C.-H. Jeong and S. H. Joo, *J. Cancer Prev.*, 2016, **21**, 13–20.

50 R. Rubbiani, S. Can, I. Kitanovic, H. Alborzinia, M. Stefanopoulou, M. Kokoschka, S. Mönchgesang, W. S. Sheldrick, S. Wölfl and I. Ott, *J. Med. Chem.*, 2011, **54**, 8646–8657.
51 W. Ma, X. Ge, L. Guo, S. Zhang, J. Li, X. He and Z. Liu, *Dyes Pigm.*, 2019, **162**, 385–393.
52 J. P. Luzio, P. R. Pryor and N. A. Bright, *Nat. Rev. Mol. Cell Biol.*, 2007, **8**, 622–632.
53 P. Saftig and J. Klumperman, *Nat. Rev. Mol. Cell Biol.*, 2009, **10**, 623–635.
54 L. He, C.-P. Tan, R.-R. Ye, Y.-Z. Zhao, Y.-H. Liu, Q. Zhao, L.-N. Ji and Z.-W. Mao, *Angew. Chem., Int. Ed.*, 2014, **53**, 12137–12141.
55 P. Boya and G. Kroemer, *Oncogene*, 2008, **27**, 6434–6451.
56 L. He, Y. Li, C.-P. Tan, R.-R. Ye, M.-H. Chen, J.-J. Cao, L.-N. Ji and Z.-W. Mao, *Chem. Sci.*, 2015, **6**, 5409–5418.
57 P. Friedl and S. Alexander, *Cell*, 2011, **147**, 992–1009.
58 S. Valastyan and R. A. Weinberg, *Cell*, 2011, **147**, 275–292.